# HWPSS Prediction for Simons Observatory and Comparisons with POLARBEAR and EBEX

Jack Lashner, Joy Didier

September 5, 2017

## Summary

In this memo we will explain our method of calculating the $n = 4$ and $n = 2$ HWPSS: $A^{(4)}$ and $A^{(2)}$. We do the calculation for both the Large and Small aperture telescopes. We will describe the methods for estimating the polarized emission and $I \to P$ for the optical elements which are dominant sources of polarized light.

Along with the Simons Observatory calculation, we also test our method on EBEX and POLARBEAR optical chains, to see how this calculation compares with the previous calculations, and the measured HWPSS of those two experiments.

## 1 $I \to P$ and Polarized Emission Calculation

The dominating sources of polarized signal seen by the detector are polarized emission from the mirrors, and $I \to P$ leakage from windows and lenses in the case of the Large Aperture Telescope, and the window and aluminum filters in the case of the Small Aperture Telescope.

### 1.1 Mirrors

From the Polarbear analysis [1] we can see that the IP leakage coefficient and the polarized emissivity of the mirrors are both given by

$$\lambda^{(4)}_{\rm opt}(\nu, \chi) = 2\sqrt{4\pi\epsilon_0\nu\rho}(\sec\chi - \cos\chi).$$

where $\rho = 2.417 \times 10^{-8}\ \Omega \cdot \mathrm{m}$ is the resistivity of the metal, and $\chi$ is the incident angle of the light with respect to the mirror normal. Here we are including the factor of 2 in the Hagen-Rubens formula which gives a better fit to data.

Our total polarized power from each mirror with incident angle $\chi$ will then be

$$P^p = \int_{\nu_{\rm low}}^{\nu_{\rm high}} \lambda^{(4)}_{\rm opt}(\nu, \chi) B(\nu, 300\ \mathrm{K}) d\nu.$$

For the time being we are ignoring the curvature of the mirrors and using a single value $\chi_{\rm ave}$ for all incident light at each mirror. We can calculate the average value of $\chi$ using the locations and focal lengths of the mirrors

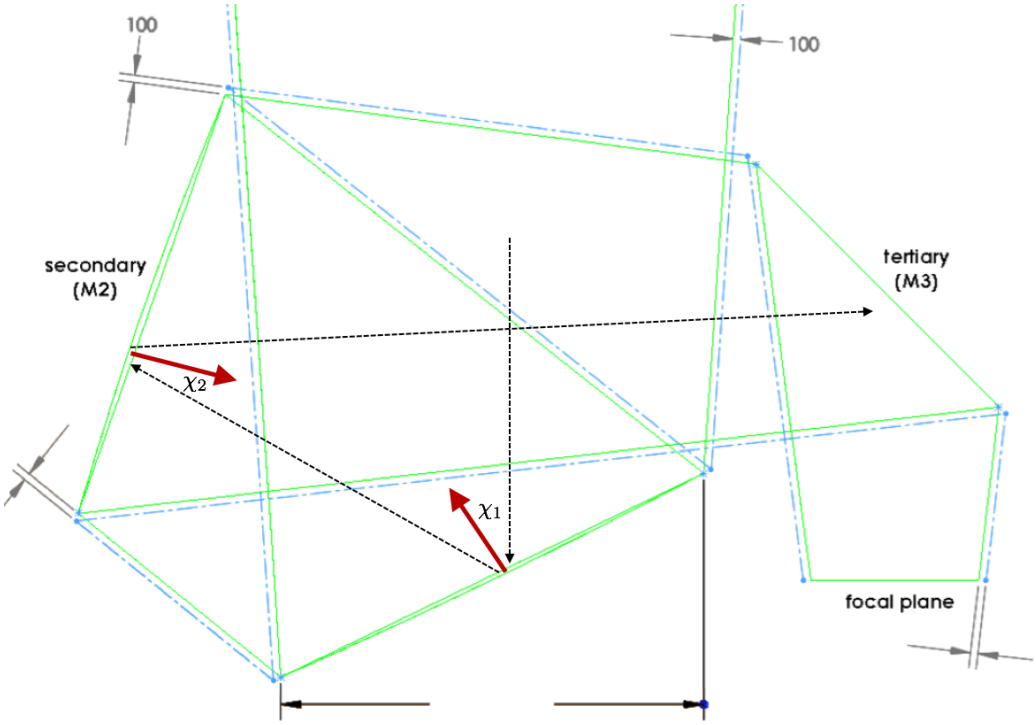


Figure 1: Above is the CCAT optical design, and the angles $\chi_1$ and $\chi_2$ for a given sample trajectory.

given in the CCAT design document. The mirror layout, and incident angles for a sample trajectory are shown in Figure 1. The average incident angles across the two mirrors are $\chi = 25.73°$ for the primary mirror, and $\chi = 19.59°$ for the secondary mirror.

### 1.2 Lenses

To estimate the $I \to P$ coefficients we use data gathered by Brian Koopman for the ACTPol telescope, by propagating unpolarized light throught the system until it reached the detector array using Code V. This is data shown in Figure 2. We can see that the $I \to P$ varies from .12% on the edge of the array to less than .015% towards the center. This simulation only takes into account the contribution for the lenses (of which there are three), so for each lens we simply dividing the total $I \to P$ by 3, which gives us .04% and .005% for the edge and center respectively.

### 1.3 Filters

Though it is not currently included in our calculation, it is also necessary to consider $I \to P$ coming from the mesh filters. The $s$ and $p$ transmission of our filters are given in [2] for incident angles of $\chi = 0°$ and $\chi = 15°$ for frequencies above 150 GHz. From the paper alone, we are able to see that the $s$ and $p$ transmissions are indistinguishable at 0°, and at 15°the maximum $I \to P$ in our desired frequency range is about .1%.

This is more than we actually expect, since the maximum incident angle in our current optical setup is around 7.5°, and this only occurs at the very edges of the beam.

Additional work is required to come up with a more realistic upper bound on the $I \to P$ .

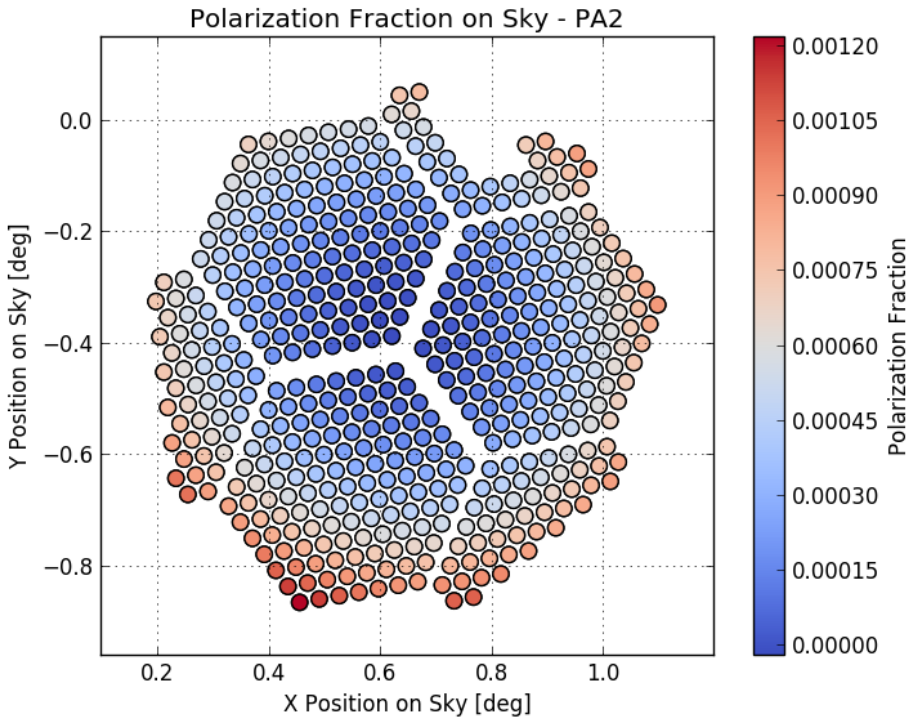


Figure 2: $I \to P$ coefficients due to lenses across the detector array of ACTPol.

### 1.4 Small Aperture $I \to P$

Unlike the large aperture system, rays hitting a given pixel enter the optics parallel to one another. Because of this a simple plane wave analysis should be reasonably accurate to calculate the IP of each element. This can be done by applying the Fresnel equations at each boundary. For stacks of thin films, this can easily be done using the transfer matrix method described in [3] using the python tmm package. We calculate the IP coefficient by taking the transmission of s and p-waves separately and calculating the polarized fraction:

$$\text{IP} = \frac{T_p - T_s}{T_p + T_s}.$$

We can then average this over the bandwidth of the detectors. The major sources of $I \to P$ leakage that we consider are the window and the two aluminum filters which are on the sky-side of the HWP.

One issue with the calculation is the presence of Fabry-Pèrot interference between filters. Because of this the IP coefficient of the two Aluminum filters is dependent on the distance between them, as seen in Figure 3. For the time being since the distances are not final, and the amplitude of the interference dies down with distance, I am simply taking the average as the distance increases and dividing the IP equally among the two aluminum filters. The $I \to P$ calculated using this method is given in Table 1

## 2 Propagation

Using this information we may propagate the power through each element. In this first iteration, if $P_n^{u/p}(\nu)$ is the unpolarized / polarized incident power on the $n^{\text{th}}$ optical element, we calculate the incident power on the

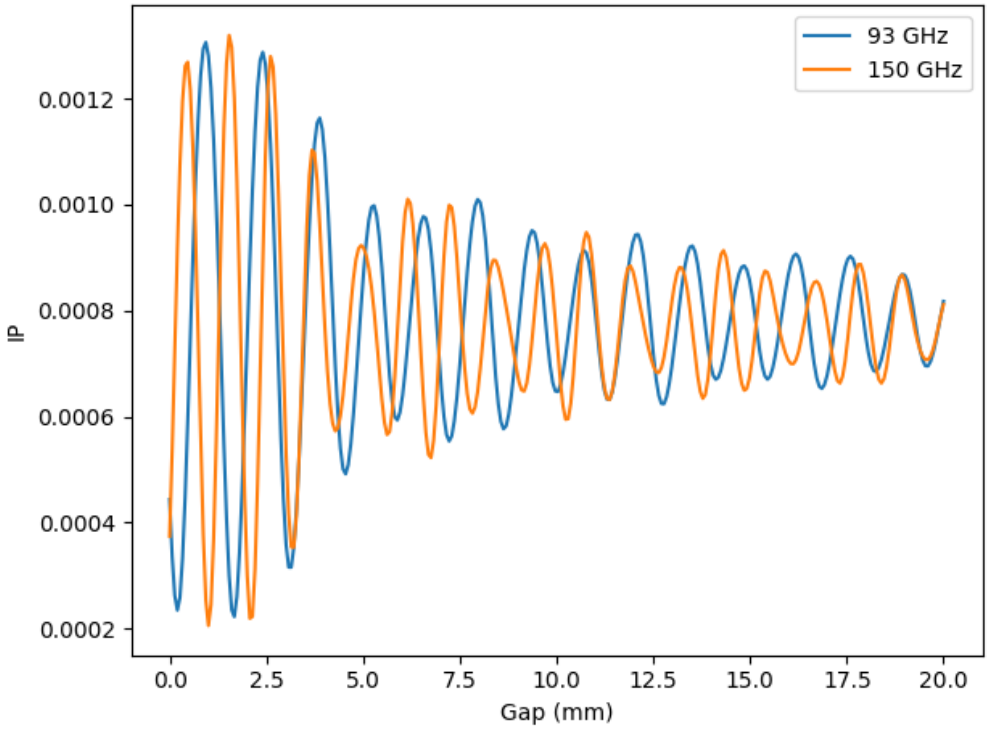


Figure 3: $IP$ coefficient as a function of distance for a system with just two aluminum filters separated by a gap. The incident angle is 7.5°, and frequencies of both 93 and 150 GHz are shown.

$(n+1)^{\text{th}}$ element as

$$P^u_{n+1}(\nu) = P^u_n(\nu)\eta^u_n(\nu)(1-\eta^{\text{ip}}_n(\nu)) + A\Omega(\nu)\,\varepsilon^u_n(\nu)B(\nu,T_n) \tag{1}$$

$$P^p_{n+1}(\nu) = P^u_n(\nu)\eta^u_n(\nu)\eta^{\text{ip}}_n(\nu) + P^p_n(\nu)\eta^p_n(\nu) + A\Omega(\nu)\,\varepsilon^p_n(\nu)B(\nu,T_n) \tag{2}$$

where $\eta^{u/p}_n$ is the unpolarized/polarized efficiency of element $n$, $\eta^{\text{ip}}_n$ is the $I \to P$ coefficient, $\varepsilon^{u/p}_n$ is the unpolarized/polarized emissivity, and $B(\nu,T)$ is the spectral brightness.

The absorption and reflection coefficients for the Large Aperture Telescope are given in the optical chain file and shown in Table 4. Additional info such as scattering and spillover coefficients are also given. Because elements are in thermal equilibrium, the absorption is equal to the emissivity $\varepsilon$. The only exception to this is the primary mirror, where spillover onto heated surfaces adds additional emissivity. The efficiency $\eta$ is then given by subtracting each coefficient from 1:

$$\eta_n = 1 - \text{abs}_n - \text{refl}_n - \text{scatt}_n$$

After the HWP, additional polarized signal no long contributes to our measurement, so the propagation of the polarized power simply becomes

$$P^p_{n+1}(\nu) = P^p_n(\nu)\eta^p_n(\nu) \tag{3}$$

To get the total unpolarized/polarized power on the detector we integrate

$$P^u = \frac{1}{2}\int_{\nu_{\text{low}}}^{\nu_{\text{high}}} P^u_{\text{det}}(\nu)d\nu, \qquad P^p = \int_{\nu_{\text{low}}}^{\nu_{\text{high}}} P^p_{\text{det}}(\nu)d\nu$$

| $\theta$ | Window IP (%) | | Aluminum Filter IP (%) | |
|---|---|---|---|---|
| | 95 GHz | 150 GHz | 95 GHz | 150 GHz |
| 7.5° | 0.069 | 0.0028 | 0.0388 | 0.0386 |
| 10.0° | 0.120 | 0.0051 | 0.0679 | 0.0703 |
| 12.5° | 0.190 | 0.0081 | 0.104 | 0.113 |
| 15.0° | 0.279 | 0.0117 | 0.147 | 0.172 |

Table 1: Above are the band averaged IP coefficients for the window and aluminum filters at 93 and 150 GHz for the Small Aperture Telescope. $\theta$ is the incident angle of the lighton the surface.

$P_{\rm det}$ is the power once the efficiency of the detector is already taken into account. $A\Omega$ is already accounted for in the propagation. The factor of 1/2 is needed when calculating the unpolarized power because we are measuring a single linear polarization, while it is not included in the polarized power since we do not know the orientation of the polarization of the incoming light, and are looking for the maximum value.

# 3 $A^{(4)}$ Calculation

## 3.1 Large Aperture Results

Since these calculations are very similar to those done in Charlie Hill's sensitivity code, our code was built to be compatible with his input files. We have run the model with the input data for the 45 cm aperture and silicon lenses for various HWP positions: between the first lense and the window, between the second and first lenses, and between the 2nd lens and the aperture. The optical chain and HWP positions are shown in Table 4. The HWPSS seen by the detector for each HWP position is shown in Table 5. The $a_4$ coefficients for various frequencies and HWP positions are given in 6.

## 3.2 Small Aperture Results

The optical chain used for the small aperture is given in table 4. The efficiency of the aluminum filters is calculated using the dielectric loss function (taken from Charlie Hill's code):

$$\text{eff} = 1 - \exp -\frac{2\pi n \delta d}{\lambda}$$

where $n$ is the index of refraction, $\delta$ the loss tangent, and $d$ the thickness of the filter. For these aluminum filters $n = 1.3$, $d = 2$ mm and $\delta = .5$. I don't quite understand how the units in Charlies code work out, because it requires $\lambda$ to be in nm.

$A^{(4)}$ for a detector at the edge of the array for various incident angles are given in Table 7. For the small aperture telescope, the f-number and FOV have not yet been decided. Because the f-number determines the aperture efficiency, changing this changes the polarized power at the detector. In order to avoid this, the power (pW) that is given is the equivalent power at the start of the telescope. That is, the total telescope efficiency has been divided out making it independent of f-number.

### 3.3 Polarbear

For a simplified comparison, we used the same optical chain as SO, but with a HWP in between the first and second mirrors. For the primary mirror we use 32.5°, as stated in [1]. At $\nu = 145$ GHz this gives us a final HWPPS of $A^{(4)}_{0|<I_{\rm in}>} = .029175$ pW. Using the conversion $\eta = .18$ pW/K, this give us 162 mK. This is consistent with the average measurements given in Table 1 of [1], which is about 160 mK.

### 3.4 EBEX

For our comparison with EBEX we use the optical chain given in Christopher Geach's memo on May 1st. In his analysis Christopher calculates the average polarization fraction across the curved mirror

$$p(\chi) = \frac{\sin^2\chi}{1+\cos^2\chi}$$

to be 15.6% for the primary mirror and 6.4% for the secondary mirror. We then solve for $\chi$ to be used in our own calculations, which gives us 31.3° and 20.3°. At 150 GHz, the $I \to P$ of the field lens is about 2.7% towards the edge of the array. Using these values we end up with $A^{(4)}_{0|<I_{\rm in}>} = .2218$ pW, which is larger than their observed value of 0.158 pW.

A possible reason for this is because 2.7% is the maximum $I \to P$ value throughout the detector. Decreasing this coefficient to 1.7% gives us $A^{(4)}_{0|<I_{\rm in}>} = .154$ pW which is much closer to the measured result.

## 4 $A^{(2)}$ Calculation

### 4.1 Calculation

Using the propagation method described in the sections above, the incident unpolarized power on the HWP plate $P^u_{\rm HWP}$ can be calculated. The HWP has a Mueller matrix :

$$M_{\rm HWP} = \begin{pmatrix} T & \rho & 0 & 0 \\ \rho & T & 0 & 0 \\ 0 & 0 & c & -s \\ 0 & 0 & s & c \end{pmatrix}.$$

The Mueller coefficients $T$, $\rho$, $c$, and $s$ at each frequency were calculated by Martina for HWPs at each frequency with an anti-reflective coating. $T$ and $\rho$ determine $A^{(2)}$ and are shown in Figure 4 at a frequency of 150 GHz.

From $M_{\rm HWP}$ we can see that the $I \to P$ coefficient and thus the polarized emissivity is given by $\rho$. $a_2$ is then calculated as the average value of $\rho$ over the detector bandwidth, and values are give in Table 2. Since emitted polarized light, and the light that is polarized through $I \to P$ are out of phase they are subtracted from one another, and the output polarized power of the HWP is given by

$$P^p_{\rm HWP+1}(\nu) = \rho(\nu)\left(P^u_{\rm HWP}(\nu) - A\Omega(\nu)B(\nu, T_{\rm HWP})\right)$$

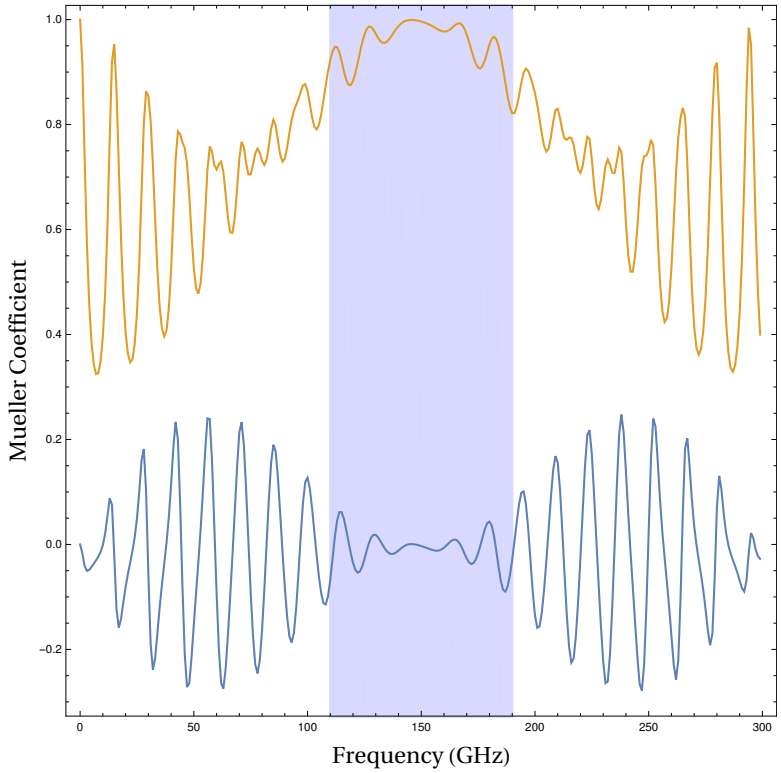


Figure 4: Shown above are the simulated Mueller elements of the HWP Mueller Matrix at 150GHz with anti-reflective coating. The orange line is T, the transmission coefficient of I and Q stokes parameters, and the blue line is $\rho$, the mixing coefficient between I and Q. The blue area is the range of the detector.

To calculate $A^{(2)}$ we then need $\eta_{\rm det}$, the combined efficiency of all elements between the HWP and the detector. We then integrate over the range of the detector to get

$$A^{(2)} = \left| \int_{\nu_{\rm low}}^{\nu_{\rm high}} \eta_{\rm det}(\nu) P^{p}_{\rm HWP+1} d\nu \right|.$$

## 4.2 Results

Result for $a_2$ and $A^{(2)}$ can be seen in Table 2

| freq (GHz) | $a_2$ (%) | $A^{(2)}$ (pW) | $A^{(2)}$ ($K_{\rm CMB}$) |
|---|---|---|---|
| 27.0 | 0.8963 | 0.0017 | 0.212 |
| 39.0 | 0.4152 | 0.004 | 0.1391 |
| 93.0 | 0.3167 | 0.0067 | 0.1413 |
| 145.0 | 0.3576 | 0.0165 | 0.2389 |
| 233.0 | 0.6395 | 0.1211 | 1.446 |

Table 2: $a_2$ and $A^{(2)}$ for the optical system given in table 4 with the HWP at 4 K. Only one position is shown because changing the position of the HWP only alters the result by about .01 fW.

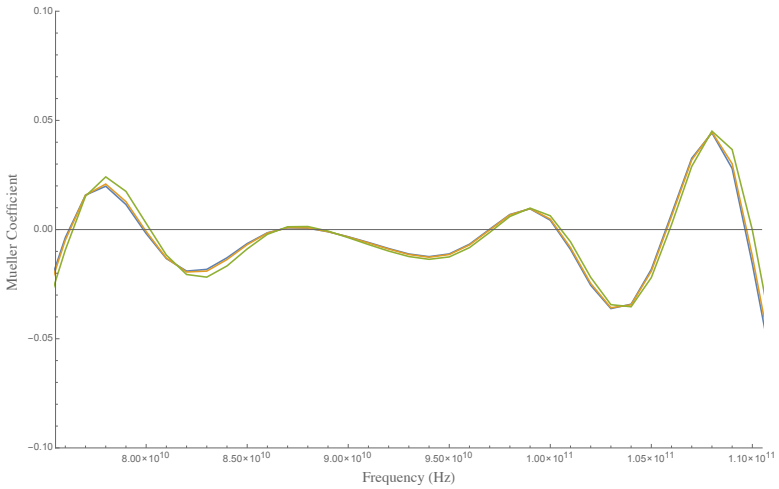


Figure 5: Shown above is the $\rho$ Mueller coefficient for incident angles of 8° (blue), 10° (orange), and 15° (green) for a band centered at 90 GHz

### 4.3 Small Aperture

The Small Aperture calculation of $A^{(2)}$ and $a_2$ is identical to that of the large aperture calculation, and the same HWP calculations are used. As we did for $A^{(4)}$, the power given in pW is the equivalent power entering the telescope rather than at the detector.

The results can be seen in Table 3. $A^{(2)}$ is mainly controlled by the HWP Mueller matrix, which doesn't change much as a function of incident angle as seen in figure 5. Based on this, the little change seen in $A^{(2)}$ makes sense.

| $\theta$ | $A^{(2)}$ (pW) | | $A^{(2)}$ ($K_{CMB}$) | |
|---|---|---|---|---|
| | 90 GHz | 150 GHz | 90 GHz | 150 GHz |
| 8° | 0.0499 | 0.0752 | 0.133 | 0.236 |
| 10° | 0.0482 | 0.0764 | 0.129 | 0.244 |
| 15° | 0.042 | 0.0866 | 0.118 | 0.272 |

Table 3: $A^{(2)}$ for the small aperture telescope for various incident angles. When the power is given in pW, it is the equivalent power entering the telescope rather than the power at the detector.

## References

[1] Satoru Takakura et al. "Performance of a continuously rotating half-wave plate on the POLARBEAR telescope". In: *Journal of Cosmology and Astroparticle Physics* 2017.05 (May 2017). arXiv: 1702.07111, pp. 008–008. ISSN: 1475-7516. DOI: 10.1088/1475-7516/2017/05/008. URL: http://arxiv.org/abs/1702.07111.

| SO Large Aperture [150 GHz, 250 GHz] | | |
|---|---|---|
| Name | Temp (K) | Abs |
| Mirror | 273 | [0.002, 0.005] |
| POLARBEAR HWP | | |
| Mirror | 273 | [0.002, 0.005] |
| Window | 265 | [0.005, 0.010] |
| HWP pos 1 (80 K) | | |
| IRShaders | 80 | [0.001, 0.001] |
| IRShaders | 40 | [0.001, 0.001] |
| LowPass | 10 | [0.010, 0.010] |
| Lens | 4.5 | [0.007, 0.011] |
| HWP pos 2 (4 K) | | |
| Lens | 1.2 | [0.007, 0.011] |
| HWP pos 3 (4 K?) | | |
| Aperture | 1.2 | NA |
| Lens | 1.2 | [0.007, 0.011] |
| LowPass | 1.2 | [0.010, 0.010] |
| LowPass | 1.2 | [0.010, 0.010] |
| LowPass | .1 | [0.010, 0.010] |

| SO Small Aperture [93 GHz, 150 GHz] | | |
|---|---|---|
| Name | Temp | Abs |
| Window | 300.0 | [0.005,0.010] |
| IRShader1 | 298.0 | [0.001,0.001] |
| IRShader2 | 293.0 | [0.001,0.001] |
| IRShader3 | 290.0 | [0.001,0.001] |
| IRShader4 | 276.0 | [0.001,0.001] |
| AluminaF | 82.00 | NA |
| IRShader1 | 76.00 | [0.001,0.001] |
| IRShader2 | 70.00 | [0.001,0.001] |
| IRShader3 | 65.00 | [0.001,0.001] |
| IRShader4 | 61.00 | [0.001,0.001] |
| AluminaF | 42.00 | NA |
| HWP | | |
| AluminaF | 40.00 | NA |
| AluminaF | 5.000 | NA |
| LowPass1 | 4.000 | [0.010,0.010] |
| Aperture | 1.000 | NA |
| Lens | 1.000 | NA |
| Lens | 1.000 | NA |
| LowPass1 | 0.100 | [0.010,0.010] |

Table 4: Our current optical chain with a 45 cm aperture and silicon lenses. Shown is also the three HWP positions which we have considered, and the HWP position used for our POLARBEAR comparison.

| | HWPSS (pW) | | |
|---|---|---|---|
| freq(GHz) | pos 1 | pos 2 | pos 3 |
| 27 | 0.00078, 0.00078 | 0.00083, 0.00079 | 0.0009, 0.0008 |
| 39 | 0.00347, 0.00347 | 0.00376, 0.00351 | 0.00414, 0.00356 |
| 93 | 0.01055, 0.01055 | 0.01125, 0.01064 | 0.01208, 0.01074 |
| 145 | 0.02605, 0.02605 | 0.02771, 0.02626 | 0.02957, 0.02649 |
| 233 | 0.08141, 0.08141 | 0.08881, 0.08234 | 0.0965, 0.0833 |

| | HWPSS ($K_{CMB}$) | | |
|---|---|---|---|
| freq (GHz) | pos 1 | pos 2 | pos 3 |
| 27 | 0.0978, 0.0978 | 0.1037, 0.0985 | 0.1125, 0.0996 |
| 39 | 0.1201, 0.1201 | 0.1301, 0.1214 | 0.1431, 0.123 |
| 93 | 0.2231, 0.2231 | 0.2379, 0.225 | 0.2555, 0.2272 |
| 145 | 0.3757, 0.3757 | 0.3996, 0.3787 | 0.4264, 0.382 |
| 233 | 0.972, 0.972 | 1.0603, 0.983 | 1.152, 0.9945 |

Table 5: Calculated $A^{(4)}_{0|<I_{\rm in}>}$ for the optical chain in table 4 at the three positions shown. In each cell, the first number is $A^{(4)}_{0|<I_{\rm in}>}$ for a detector towards the edge of the array, and the second number is for a detector towards the center. We present the power in both pW and $K_{CMB}$

| | $a_4$ | | |
|---|---|---|---|
| freq (GHz) | pos 1 | pos 2 | pos 3 |
| 27 | .00017 | .00057 | .00097 |
| 39 | .00021 | .00061 | .00101 |
| 93 | .00032 | .00072 | .00113 |
| 145 | .00041 | .00081 | .00121 |
| 233 | .00052 | .00092 | .00132 |

Table 6: $a_4$ of the system, including the contribution from the two mirrors and the lenses on the sky side of the HWP.

| $\theta$ | $A^{(4)}$ (pW) | | $A^{(4)}$ ($\mathrm{mK_{CMB}}$) | |
|---|---|---|---|---|
| | 90 GHz | 150 GHz | 90 GHz | 150 GHz |
| 7.5° | 0.226 | 0.047 | 0.604 | 0.149 |
| 10° | 0.404 | 0.086 | 1.08 | 0.270 |
| 12.5° | 0.636 | 0.138 | 1.70 | 0.433 |
| 15° | 0.929 | 0.208 | 2.48 | 0.653 |

Table 7: $A^{(4)}$ for the small aperture telescope for various incident angles. When the power is given in pW, it is the equivalent power entering the telescope rather than the power at the detector.


[2] Giampaolo Pisano, Peter A. R. Ade, and Samuel Weaver. "Polarisation effects investigations in quasi-optical metal grid filters". In: *Infrared Physics & Technology* 48.2 (June 1, 2006), pp. 89–100. ISSN: 1350-4495. DOI: 10.1016/j.infrared.2005.04.004. URL: http://www.sciencedirect.com/science/article/pii/S1350449505000526.

[3] Thomas Essinger-Hileman. "Transfer matrix for treating stratified media including birefringent crystals". In: *Applied Optics* 52.2 (Jan. 10, 2013), p. 212. ISSN: 0003-6935, 1539-4522. DOI: 10.1364/AO.52.000212. arXiv: 1301.6160. URL: http://arxiv.org/abs/1301.6160.